International Journal of Mechanical Engineering and Applications
2019; 7(1): 8-16
http://www.sciencepublishinggroup.com/j/ijmea
doi: 10.11648/j.ijmea.20190701.12
ISSN: 2330-023X (Print); ISSN: 2330-0248 (Online)

Numerical Estimation of Heat Recovery within a Distributed Incinerator Using Water and Hydrocarbons as Working Fluids

Hikaru Yamashiro[1, *], Tomoyasu Yara[1], Kenji Fukutomi[2]

[1]National Institute of Technology, OKINAWA College, Nago, Japan

[2]THOMAS Technical Research Company, Uruma, Japan

Email address:

hyama@okinawa-ct.ac.jp (H. Yanashiro)

[*]Corresponding author

To cite this article:

Hikaru Yamashiro, Tomoyasu Yara, Kenji Fukutomi. Numerical Estimation of Heat Recovery Within a Distributed Incinerator Using Water and Hydrocarbons as Working Fluids. *International Journal of Mechanical Engineering and Applications.* Vol. 7, No. 1, 2019, pp. 8-16.
doi: 10.11648/j.ijmea.20190701.12

Received: January 7, 2019; **Accepted**: March 13, 2019; **Published**: April 3, 2019

Abstract: The potential of a cogeneration system combined with a small combustion furnace was investigated in this study. The heat transfer between the exhaust gas and working fluid flowing in a spiral tube heat exchanger was estimated numerically and the amount of vapor generated was predicted. The combustion chamber had a 0.49 m^3 inside volume with a chimney height of 2.5 m and an inner diameter of 0.28 m. A uniform gas side temperature condition that was referenced from the results of a preliminary experiment and a computational fluid dynamics simulation were adopted to simplify calculations and clarify the effects of working fluids. The amounts of heat recovery when utilizing water and other types of working fluids (Pentane, Butane) were compared. The most effective tube length considering pressure drop and phase change was also predicted. Isentropic theoretical thermal efficiency and T-s diagrams are analyzed to evaluate the vapor-power conversion rate using waste heat. As a result, a potential the heat recovery rate of approximately 100 kW at a 150 kg/h mass flow rate is expected.

Keywords: Heat Transfer, Thermal Recycle, Incinerator, Working Fluids, Cogeneration System

1. Introduction

The practical use of cogeneration systems supplying both electric power and hot waste have been gradually increasing, especially in large-scale combustion facilities [1]. On the other hand, for relatively small incinerator having furnace volume of 1 m^3 or less, it has been considered that there are several obstacles to their practical use as cogeneration system, such as a lack of exhaust heat, instable power generation, and low economic benefit, so on. However, in recent year, the high temperature type incinerator having several forced combustion burners have been developed, and these are expected to be make practical use as a heat recovery system so called "micro-cogeneration". Therefore, the reasonable thermal design with applicable numerical estimations are crucial due to make discussions on the potential of these combustion equipment [2-3].

Previous studies regarding heat recovery can be classified into three major categories: those focused on heat exchangers [4-8], working fluids [9], and system performance [10-11]. The qualitative classification of waste heat is performed based on temperature levels of approximately 373 K and 523 K as reference values. On the other hand, regarding the thermal design of heat exchangers, heat transfer with phase change and/or two-phase flow have been attracting in academic field for long time. For recent instance, the studies dealing with two-phase flow model and numerical simulation inside porous media are presented [12-15]. These studies also help to understand heat transfer enhancement process and give the methodology for the development of latent heat recovery system with phase change process.

In industrial fields on the refrigeration and air conditioning systems, methodology of thermal design of equipment such as the evaporators and condensers have already been established [2, 3]. However, when dealing with high-temperature exhaust gas, the heat exchanger for heat

recovery introduces the problem of decreased performance because of high-temperature corrosion, deposit layers, and so on practical issues. In many cases, the volumetric flow-through-type heat exchangers have been utilized considering in the effect of radiation heat transfer in large-scale combustion furnaces [4]. In present study, spiral tube-type heat exchanger is focused, since it considered to be applicably installed into the narrow space in the small-type incinerator.

The heat recovery systems are recently investigated with focusing on waste heat below 373 K. For example, evaluation of the heat transfer performance of a spiral capillary tube is performed by Yamashita and Utaka [5], analyzed heat recovery in the heat exchanger of a regenerative steam cycle [6-10]. And the investigation in order to obtain the optimal working fluids are performed by the comparisons of Rankin cycle on the equilibrium-state diagrams [11]. However, there have been few studies focusing on quantitative verification utilizing practical data.

Based on the above research review, the potential of cogeneration system combined with the forced-combustion incinerator (view Figure 1) have been discussing in this study. As a first step, this paper presents the results of numerical estimation on heat transfer between the working fluid flowing inside a spiral tube with a pressure drop and the uniform gas side temperature. Discussion regarding the effects of working fluids for the heat recovery rate and the isentropic theoretical power conversion rate is also included.

Figure 1. *Forced combustion type incinerator.*

2. Outline of Incinerator

2.1. Dimensions and Features

Figure 1 shows a snap shot of the forced combustion incinerator developed by Thomas Co., Ltd. The combustion chamber has a 0.49 m^3 inside volume with a chimney height of 2.5 m, and it's inner and outer diameter of 0.28 and 0.3 m respectively. Waste materials in the chamber are burned by a main burner. The secondary burner is utilized to re-burn the generated gas. Additionally, fresh air is supplied from the duct through nozzles to enhance combustion. These combustion and exhaust processes effectively reduce the amounts of dioxins until less than 2.5 ng/m^3N in the exhaust gas. Measurements of temperature and the concentrations of exhaust gases, as well as the efficient control of combustion and gas cooling are performed. Preliminary experiments revealed that the temperature in the furnace reached a quasi-steady state after 20 min with relatively large-scale temperature fluctuations between 200°C and 300°C near the inside wall of the combustion furnace.

2.2. Temperature Distribution

Initially, the temperature distribution in the furnace was investigated by utilizing simulation software (Fluent 6.2). Figure 2 presents the results of temperature distributions at the quasi-steady combustion state. This calculation was performed using finite element method (number of elements and contacts: 94,237 and 61,054), based on the k-ε turbulence model. A certain volume of heat source as generation terms was placed at the lower left side in the furnace. The temperature of the heat source was given to be around 1100°C. The generated gas from the heat source was reheated by the secondary burner at the inlet of chimney where modeled as the secondary heat source terms of temperature around 900°C. The air flow supplied from the nozzles (hole) on the duct surface were given at 20 m/s. As the boundary condition, the heat transfer between the wall and outside air assumed to be constant at 60 kw/m^2K, [2]. And these assumed values as the boundary and/or initial conditions were modified to be approximately approach to the gas temperature measured utilizing the thermocouples installed in the vicinity of the inner wall.

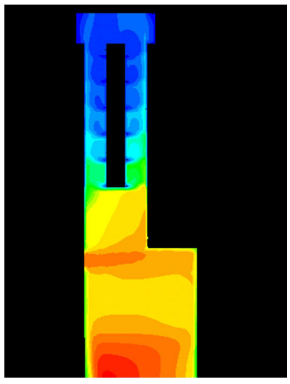

Figure 2. *Temperature distribution in incinerator.*

The temperature profile shows that the waste continued burning at temperatures between 1,100°C and 700°C without continued operation of the main burner and the exhaust gas was re-burned at approximately 800°C by a secondary burner at the exit of the chamber. The generated gas is cooled rapidly by a spray nozzle installed near the entrance of the duct installed in the chimney. Next, the exhaust gas rises in the chimney as the temperature decreases based on air injections from the duct. The exhaust temperature into the

outside air is approximately 200°C. The velocity of the exhaust gas in the chimney was estimated to be approximately 2 - 3 m/s. The dimensions of the furnace are summarized in Table 1, where the notation corresponds to Figure 3 shown in the next section.

Table 1. *Dimensions of incinerator.*

Chimney [m]	H	D_i	D_o	y_0
	2.5	0.28	0.3	0.05
Chamber [m]	h	a	b	c
	1.6	0.7	0.7	1.0

3. Numerical Calculation

3.1. Heat Transfer Model and Coordinates

Figure 3 presents the schematics of a combustion furnace with a heat exchanger. On the right side, enlarged view of heat and mass transfer model for an element of a spiral tube represented. A single stain-less steel pipe (SUS430) forms a spiral along the inner wall of the chimney of the combustion chamber. The working fluid supplied through the tube inlet flows at a constant mass flow rate M_f according the equation of continuity. The inside d_i and outside d_o tube diameters are 10 mm and 12 mm, respectively.

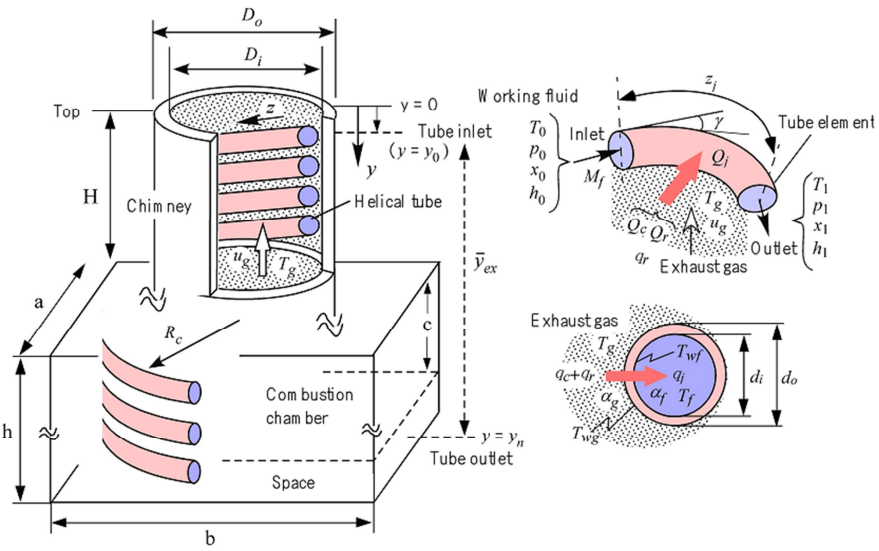

Figure 3. *Combustion furnace with spiral tube, and heat transfer model and coordinates.*

The heat and mass balance for the element of the spiral tube is expressed as

$$Q_j = M_f (h_1 - h_0) \tag{1}$$

where h is the specific enthalpy of the working fluid and Q_j is the heat transfer rate from the exhaust gas to the working fluid across the tube wall element with the number "j". The subscripts 0 and 1 represent inlet and outlet of the tube element, respectively. The Q_j for the steady state is expressed as

$$Q_j = \alpha_f (T_{wf} - T_f) \pi d_i z_j \tag{2}$$

$$Q_j = 2\pi z_j \lambda (T_{wg} - T_{wf}) / \ln(d_o / d_i) \tag{3}$$

$$Q_j = Q_c + Q_r = \left\{ \alpha_g (T_g - T_{wg}) + \varepsilon a \sigma (T_g^4 - T_f^4) \right\} \pi d_o z_j \tag{4}$$

where α is the heat transfer coefficient, and λ is the thermal conductivity. The subscripts "w", "f", "g" and "i" refer to the *wall*, *fluid*, *gas*, and *inside* respectively. And subscripts "*wf*" and "*wg*" refer to the wall at gas side and the wall at working fluid side respectively. The values of α_f and α_g obtained from the correlation equations proposed by Dittus-Boelter and Chen referred in [2]. The Q_j is represented by the sum of the convection and radiation terms Q_c and Q_r respectively in the gas side, as shown Eq. (4). The ε and a are the emissivity and absorptivity values for the radiation heat transfer on the gas side, respectively, and σ is the Boltzmann constant.

Temperature of working fluid T_f represents the arithmetic average value evaluated by Eq. (5).

$$T_f = \frac{1}{2}(T_{f0} + T_{f1}) = T_{f0} + \frac{1}{2}\Delta T_f \tag{5}$$

where the subscripts f, 0 and 1 refer to the *fluid*, *inlet* and *outlet* for the tube element, respectively.

The exhaust gas temperature of T_g is given by an approximate equation that is evaluated based on the results of computational fluid dynamics simulations (see Figure 2). This equation is defined as

$$T_g(y) = c_n y^n \tag{6}$$

where the coefficients c_n (n =0,1,2,3) take on different values depending on the combustion state in the chamber. The vertical coordinate y can be transformed into the spiral coordinate z along a tube length with the spiral angle γ, as the equation $y = y_j = z_j \sin\gamma$. In this study, to clarify the effects of a several kinds of working fluids on heat transfer characteristics, the temperature distributions on the gas side

were simplified as eq. (6). The emissivity ε and absorptivity a of the gas side were set to the maximum values of $\varepsilon = a = 1$. Table 1 present the temperature coefficients c_n which obtained in the preliminary experiment when the incinerator keeped at the steady state without gas cooling by the air nozzles. In this study, the gas side's temperature was used these values of cn for the assumption of gas side's temperature as boundary condition.

Table 2. *Values of c_n at the steady state in combustion.*

n	c_0	c_1	c_2	c_3
3	498.5	52.72	13.03	0.086

3.2. Pressure Drop

The pressure drop of the working fluid along the tube element's inside wall can be expressed as

$$\Delta p_j = p_0 - p_1 = \frac{\rho_f}{2}\left\{\left(\frac{\rho_0}{\rho_1}\right)^2 - 1\right\}u_0^2 + \rho_f g(y_0 - y_1) + \Delta p_l \quad (7)$$

where Δp_j is the element's total pipe loss sum of friction loss and curved pipe loss. And where ρ, u and g represent density, velocity and gravitational acceleration. And subscript "0" and "1", respectively. This value therefore can be expressed as

$$\Delta p_l = \rho_f g(\Delta z_b + \Delta z_f) = \frac{\rho_f}{2}\left(f_j \frac{z_j}{d_i} + \zeta_j\right)u_0^2 \quad (8)$$

where f_j is the pipe friction coefficient and ζ_j is the curved pipe loss coefficient for the tube element. These values are given by the correlation equations proposed by Ito et al. [1].

3.3. Calculation Procedure

Calculation is performed in series of tube element based on the boundary conditions of B. C. $r = r_o$: $T = T_g$, $z = z_0$, z_1: $M_{f0} = M_{f1}$ (constant mass flowrate).

The values (p_0, T_{f0}, M_f) of working fluid at the entrance to the tube where corresponds to the top of chimney and the temperature difference ΔT_f (=0.1K) are given as the initial conditions. The obtained values of T_{f1} and/or T_f (by eq.5) and p_1 are utilized for the calculation of the thermal properties. The thermal properties are obtained from the subroutine program in the NIST Ref-Prop Ver. 9 [12].

The enthalpy at the inlet h_0 (p_0, T_{f0}) and outlet h_1 (p_1, T_{f1}) are also utilized in these calculations. Q_j can be estimated from Eqs. (1) and (5), where the unknown values T_{wg}, T_{wf}, and z_j (j = 1) are given by Eqs. (2) through (6). Based on the calculated values, the thermal properties of working fluid are then the recalculated and all unknown values are calculated to derive a final solution. These calculation procedures perform sequentially from j = 1 until n, where the desired superheated vapor can be obtained. Regarding the transition of the phase change, the temperature difference between the calculated value of T_{f1} and the saturation temperature of T_{s1} was less than 0.001 (i.e. T_{s1} - T_f < ± 0.001). These values represent the boiling incipience point and dry out point, respectively. Therefore, the three heat transfer regions can be specified by $T_{f1} < T_{s1}$ for the compressed liquid, $T_{s1} = T_{f1}$ for two-phase transfer, and $T_{s1} < T_{f1}$ for the superheated vapor.

The calculation in the two-phase region ($T_{f0} = T_{f1}$), the quality at the inlet x_0, and Δx are given as initial conditions. The outlet x_1 and Q_j are calculated sequentially, similar to the above calculations. The enthalpy h_1 was defined as

$h_1 = (1 - x_1)h' + xh'' = h' + x_1 r$, where h' and h'' refer to the saturation liquid and saturation vapor, respectively. Next, the unknown values were calculated utilizing the procedure described above. The calculations proceed from the saturation liquid (x_0 = 0) to the saturation vapor (x_1 = 1), which represents the end of the two-phase region. The values of h' and h'' are based on the saturation temperature T_{s1} for the calculated outlet pressure p_1.

3.4. Overall Heat Recovery Rate and Tube Length

The overall tube length of the heat exchange Z_{ex} is defined by Eq. 9. The overall heat recovery rate Q_h, and the pressure drop Δp_{ex} along Z_{ex} are also defined by Eq. (9).

$$Z_{ex} = \sum_{j=1}^{n} z_j\ ,\ Q_h = \sum_{j=1}^{n} Q_j\ ,\ \Delta p_{ex} = \sum_{j=1}^{n} \Delta p_j \quad (9)$$

n corresponds to the end of tube, where the working fluid has reached the desired temperature or super heat ΔT_{sup}. The pressure drop per unit length is defined by

$$\Delta \bar{p}_{ex} = \Delta p_{ex} / Z_{ex} \quad (10)$$

The vertical coordinate y_n of the nth tube element of the spiral-wound single tube is expressed in terms of the length z_j and spiral angle γas

$$y_n = y_0 + \sum_{j=1}^{n} z_j \sin\gamma \quad (11)$$

where y_0 is the vertical distance of the tube's entrance from the top of the chimney as shown Figure 3. Therefor the overall tube length of heat exchanger is expressed as y_{ex},

$$y_{ex} = \sum_{j=1}^{n} z_j \sin\gamma = N\pi(D_i - d_o)\tan\gamma \quad (12)$$

where D_i is the inner diameter of the chimney, d_o is the outer diameter of the tube, and the N is the number of turns along the total tube length. The spiral tube angle is defined by the following equations.

$$\gamma = \tan^{-1}\left(\frac{d_0/2}{2R_c}\right) \text{ or} \quad (13)$$

$$\gamma = \tan^{-1}\left(\frac{d_0/2}{D_i}\right)\ Z_{ex} = H/\sin\gamma\,, \quad (14)$$

$$Z_{ex} = h/\sin\gamma \quad (15)$$

As shown Figure 3, based on the assumption that the spiral tube for the heat exchanger runs from the near top of the chimney to the bottom of the combustion chamber, Z_{ex} is geometrically defined as the maximum tube length $Z_{ex,max}$ of a perfect circular coil without gaps.

The dimensions of the spiral tube and the initial conditions are summarized in Table 3 and 4.

Table 3. *Dimensions of spiral tube.*

Material	d_o [mm]	d_i [mm]	γ[deg.]
Sus430	12.0	10.0	1.0

Table 4. *Initial conditions of working fluid.*

Kinds	T_{f0} [K]	M_f [kg/h]	p_0 [MPa]
Water Butane Pentane	300	10-150	2.0

4. Numerical Results

4.1. Tube Length and Amount of Heat Recovery

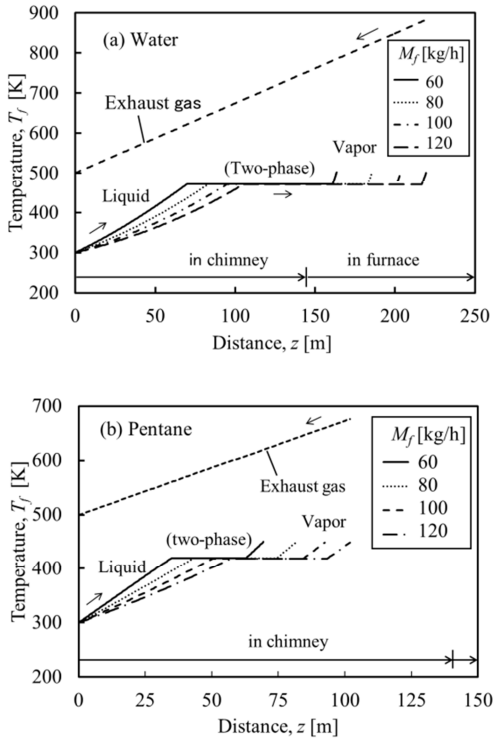

Figure 4. *Changes in temperature of working fluid: (a) Water, (b) Pentane.*

The estimation of the transition points in the phase change process is crucial on the thermal design of the heat exchanger. Figure 4 present the temperature changes in the working fluid in a single spiral tube with a constant mass flow rate M_f ranging from 60 - 120 kg/h. The effects of working fluid can understand by comparisons between Figure 4(a) and (b) for water and pentane, respectively. The dotted lines in the figures represent the variation in the gas side temperature by assumption utilized the temperature distributions in Figure 2. Initially, T_f increases gradually, then remains nearly constant in the two-phase region, and finally increases gradually again in the gas phase region. This tendency of the temperature profile is similar for both water and pentane. This calculation is useful for estimating the transition of the phase change in spiral tube.

The distance to the transition of the phase change moves toward the down-flow side with an increasing M_f. This means that a longer heat transfer distance is required to obtain the larger amount of desired superheated vapor. In the case of water, the tube outlet reaches a distance of more than 150 m and is located inside the combustion chamber through chimney. In case of pentane, the outlet reaches a relatively short distance compared to water and is located inside the chimney.

Figure 5(a) and (b) present comparisons of the overall heat recovery Q_h for water and pentane flowing with the same M_f. The notation Q_h in the bar graph refers to the integrated values in the liquid phase region, two-phase region, and gas phase region, respectively. Q_h increases nearly linearly with an increasing M_f for both water and pentane.

The Q_h ranges from 45 - 95 kW for water and 10 - 20 kW for pentane, which indicates that the heat recovery rate of water is approximately 4.5 times that of pentane in the M_f range of 45 - 95 kg/h. The ratios of heat recovery in the two-phase region for water and pentane are approximately 72% and 39%, respectively. This means a relatively larger heat recovery rate is obtained in the two-phase region for water with large latent heat.

Figure 6 presents comparisons of the overall tube lengths Z_{ex} for three types of working fluids: water, pentane, and butane. The vertical axis in the graph represents both the Z_{ex} and y_{ex} axis for the spiral tube heat exchanger. Z_{ex} corresponds to the estimated distance to the outlet to obtain the desired superheated vapor of 50 K. Z_{ex} increases nearly linearly with increasing M_f. For an example at M_f = 120 kg/h, Z_{ex} represents 220 m for water, 102 m for pentane, and 88 m for butane. Z_{ex} shows significant differences between working fluids.

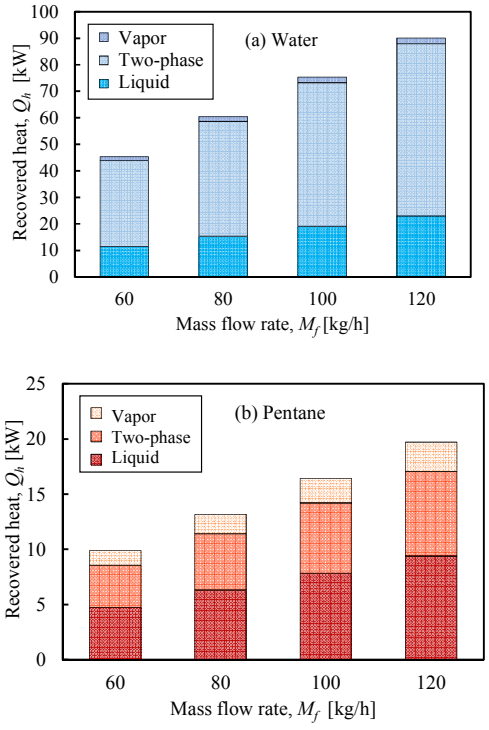

Figure 5. *Amount of recovered heat with changing mass flow rate: (a) Water, (b) Pentane.*

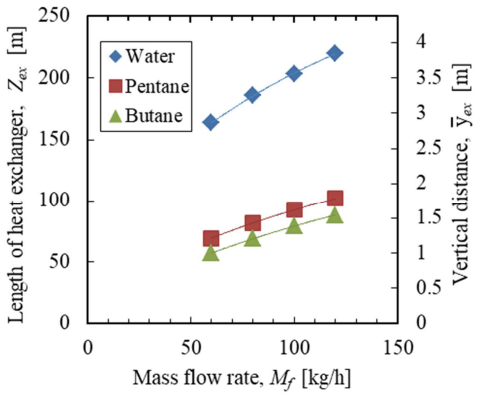

Figure 6. *Comparisons of overall tube length.*

4.2. Pressure Drop in Tube

Figure 7 presents comparisons of pressure drops per unit length in the helical tube for three types of working fluids. Δp_{ex} increases nearly linearly with M_f with same tendency for water, pentane and butane, respectively. The Δp_{ex} values for pentane and butane are 27-30% lower than that for water. The difference of the working fluid increases at high flow rate.

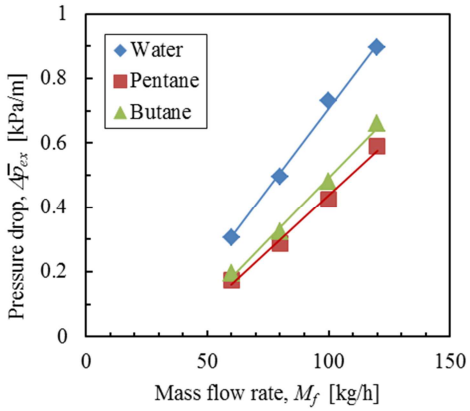

Figure 7. *Pressure drop per unit tube length.*

4.3. T-s Diagram and Theoretical Thermal Efficiency

In order to make a discussion on the potential of the heat recovery-power conversion system, here virtually considers a Rankine cycle combined with this incinerator. Figure 8(a) and (b) present comparisons of the Rankine cycles on the *T-s* diagrams for two kinds of working fluids of water and pentane, respectively. The superheated vapor obtained by the heat recovery (point h_4) expands adiabatically to the condensation temperature of T_c = 310 K, and the maximum theoretical work $L_{th} = M_f (h_4 - h_5)$ value can be obtained during this process. In the case of water, the superheated vapor at the state h_4 is considered to enter into the two-phase flow during this process, and it reaches the state of point h_5 where the water vapor corresponds to the saturation pressure p_c for T_c. In the case of pentane, the superheated vapor at h_4 reaches h_5 as the superheated vapor corresponding to the p_c for T_c and then decreases in temperature until it reaches the point h''_5 of saturated vapor on the isobaric line ($p = p_c$). From these comparisons of *T-s* diagrams, it's obvious that the adiabatic heat drop Δh_{ad} of water vapor is significantly larger than that of the pentane vapor.

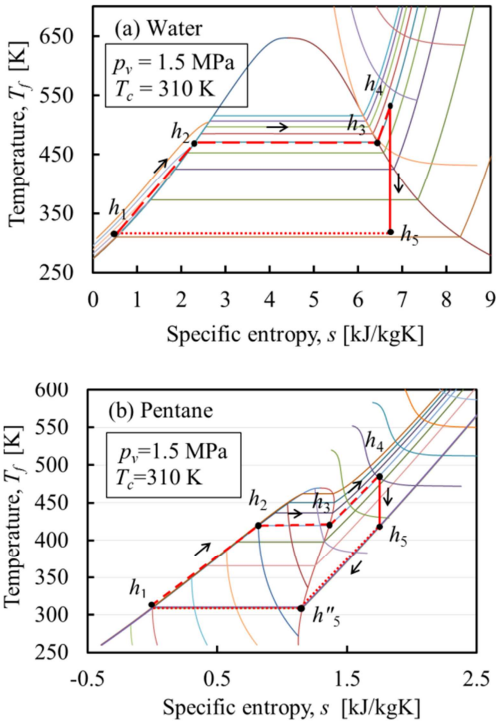

Figure 8. *Comparison of Rankine cycles on T-s diagram: (a) Water, (b) Pentane.*

The theoretical thermal efficiency η_{th} is defined by $\eta_{th} = (h_4 - h_5) / (h_4 - h_1)$ and utilizes the specific enthalpy values $h_{1\text{-}5}$ of each state. Figure 9 presents the effects of condensation temperature on theoretical efficiency. The η_{th} for water ranges from 35 to 30 % in a T_c range of 280-320 K, decreases gradually as T_c increases. The difference in thermal efficiency between different working fluids is clearly visible.

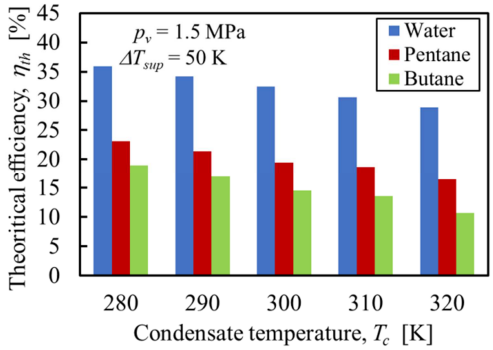

Figure 9. *Variation of theoretical thermal efficiency with condensate temperature.*

Figure 10 presents the effects of evaporation pressure p_e on η_{th} and compares three types of working fluids. η_{th} shows a tendency to slightly increase as p_v increases. To summarize the information in Fig.9 and 10, the η_{th} is higher in the order of water, pentane, and butane. These ranges are 28 - 36% for water, 15 - 23% for pentane, and 10 - 18% for butane in the pv ranges 1-2 MPa.

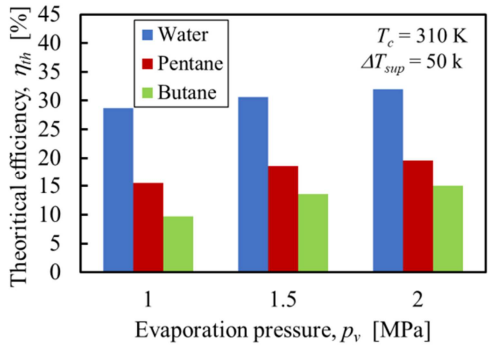

Figure 10. *Variation of theoretical thermal efficiency with evaporation temperature.*

4.4. Maximum Heat Recovery and Power Conversion

By substituting the dimensions (d_o = 12 mm, D_i = 280 mm, H = 2.5 m, h = 1.6 m) into the Eqs. (13) - (15), the maximum tube length $Z_{ex,max}$ installable in the furnace can be estimated to be 299 m, with 116 m in the chimney and 183m in the combustion chamber. Considering the obstacles and corners in the actual piping, the maximum tube length within this furnace is considered to be reasonably $Z_{ex,max}$ = 250 m.

Figure 11 presents the comparison of Q_h for three types of working fluids with the M_f range 0-150 kg/h in a single tube length of 250 m. The amount of critical heat recovery rate within the chimney is approximately expressed by the dotted line in this figure. In the case of water, Q_h gradually increases with M_f and reaches a maximum value around M_f = 150 kg/h. This means that the tube end for water cannot reach the desired superheated vapor at M_f > 150 kg/h because the tube length has already reached the maximum. In contrast, in the case of pentane and butane, Z_{ex} has not reached the maximum length and Q_h has not reached the critical value. Hence a much larger amount of superheated vapor can be expected to be recovered in using pentane and butane.

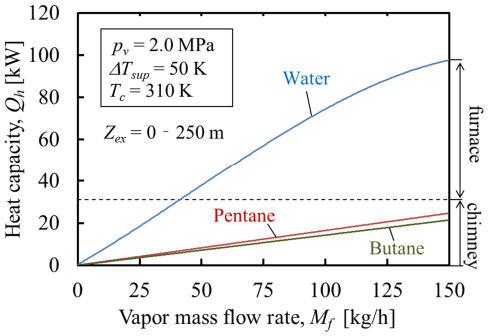

Figure 11. *Variation of heat capacity with mass flow rate.*

As described in Figures 9 and 10, assuming the average thermal efficiencies η_{th} of each working fluid are 30% for water, 16% for pentane, and 12% for butane, the maximum adiabatic recovery work can be estimated as $L_{ad} = \eta_{th}\ Q_h$. Additionally, if the external efficiency η_p of the turbine-linked generator is given, the electric power can be approximately estimated as $E_p = \eta_p\ L_{ab}$.

Figure 12 presents the changes in L_{ad} and E_p with respect to M_f and compares of three types of working fluids. η_p was given as 30% refer to [8] and [9]. L_{ad} and E_p increase with M_f, similar to the trend in Fig11. An electric power generation of 11 kW is estimated at a flow rate M_f = 150 kg/h when water is utilized as the working fluid. In contrast, the E_p values for pentane and butane are less than 2 kW at M_f = 150 kg/h. However, E_p have not reached the maximum values under this condition.

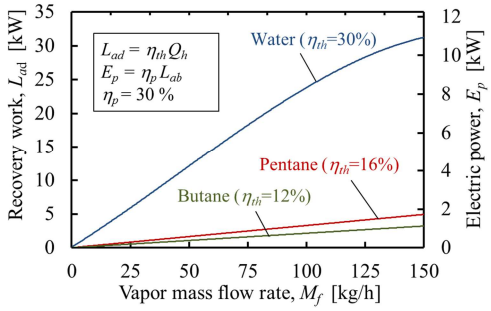

Figure 12. *Variation of recovery work and electric power with vapor mass flow rate.*

5. Conclusions

This study focused on the potential of a micro cogeneration system by estimating the recovered heat from a combustion furnace of a predetermined size. Numerical calculations were performed based on the heat transfer model between the exhaust gas and working fluid assume to use a spiral tube heat exchanger. The key findings from this study are as follows.

(1) When a smooth tube with a diameter of 12 mm is installed in the form of a spiral along the inner wall of the test furnace shown Figure 1, an overall tube length around 250 m can be piping for the heat exchanger.

(2) Utilizing water as a working fluid, the heat recovery rate was estimated to be approximately 100 kW (31 kW in chimney, 69 kW in fire chamber) at a constant flow rate of 150 kg/h with a tube of length 250 m.

(3) If the Rankine cycle is operated with the obtained superheated vapor at p_v = 1.5 MPa and T_c = 310 K, the theoretical thermal efficiency η_{th} ranges from 28 - 36% for water, 15 - 23% for pentane, and 10 - 18% for butane.

(4) Assuming that the external efficiency η_p is 30%, the amount of electric power generation can be approximately estimated as 11 kW for water and less than 2 kW for pentane and butane at the same M_f value of 150 kg/h.

(5) The pentane and butane have desirable characteristics as working fluids for heat recovery and dissipating heat with a small temperature difference in narrow spaces because of their lower pressure drops and lower saturation temperatures.

(6) To assess the above conclusions, the experimental investigation should be performed with practical application.

Acknowledgements

The authors thank for the support of the Okinawa

Prefecture Science and Technology Innovation Project in 2017-2018. We also appreciate the coordinating of Dr. Y. Nagawa and Dr. I. Matsui of the Okinawa Science and Technology Promotion Center.

Nomenclature

a, b, c, h, H	dimensions of combustion furnace [m]
c_n	gas temperature coefficient [-]
d	tube diameter [m]
D	diameter of chimney [m]
g	gravitational acceleration [m/s^2]
h	specific enthalpy [J/kg]
M	mass flow rate [kg/s] or [kg/h]
N	number of turn [time]
p	pressure [Pa]
Δp	pressure drop [Pa]
Q	heat transfer rate [W]
q	heat flux [W/m^2]
R_c	coil radius of spirally wound tube [m]
s	specific entropy [J/(kg·K)]
T	temperature [K]or[°C]
u	velocity [m/s]
x	quality of working fluids [—]
y	vertical coordinate or vertical head [m]
$\bar{y}$	distance or length [m]
Z	overall tube length [m]
z	spiral coordinate or length of element [m]
Δz_b	bending loss head of tube element [m]
Δz_f	friction loss head of tube element [m]
α	heat transfer coefficient [W/(m^2·K)]
ε	emissivity [—]
a	absorptivity [—]
λ	thermal conductivity [W/(m·K)]
σ	Stefan-Boltzmann constant [W/(m^2·K^4)]
γ	spiral angle [rad.]
ρ	density [kg/m^3]

Subscript

ad	adiabatic
b	boiling
c	convection
ex	heat exchanger
f	working fluid
g	gas or gas side
i	inside or inner
j	element's number
l	loss
o	outside
p	power
r	radiation
w	wall
wg	gas side's wall
fg	fluid side's wall
0	inlet
1	outlet

References

[1] Takuma Co., Ltd., Environmental Technology Research Association, "Waste Incineration Technology", *Ohm-Sha*, 2010, pp. 1-200.

[2] The Japan Society of Mechanical Engineers, *Heat Transfer Data Book 5 th ed*., 2009, pp. 105-204.

[3] The Japan Society of Refrigerating and Air Conditioning Engineers, *Refrigeration*, Special ed., Vol. 090, No. 1047, 2015, pp. 3-22.

[4] R. Echigo, K. Hanamura, Y. Takahashi, M. Okuyama, S. Jugjai, A. Hagiwara, Y. Usami and N. Funahashi, "Heat transfer analysis for a tubular methane-steam reformer with a porous radiative converter", *Transactions of the Japan Society of Mechanical Engineers*, Series B, Vol. 57, No. 539, 1991, pp. 163-169.

[5] J. Yamashita and Y. Utaka, "On prediction of heat exchanger performance for latent heat recovery using flue gas", *Transactions of the Japan Society of Mechanical Engineers*, Series B, Vol. 80, No. 818, 2014, pp. 1-14.

[6] A. S. Hegazy, "Possible waste heat recovery in the condenser of a regenerative steam cycle", *Journal of Thermal Science and Technology*, Vol. 2, No. 1, 2007, pp. 1-12.

[7] H. Takamatsu, H. Yamashiro, N. Takata, H. Honda, "Vapor absorption by LiBr aqueous solution in vertical smooth tubes", *International Journal of Refrigeration*, Vol. 26, 2003, pp. 659-666.

[8] Le Minh Nhut, Young-Sub Moon, Youn Cheol Park, "A study on energy optimization of heat exchanger in a gasification system", *International Journal of Mechanical Engineering and Applications*, Vol. 4, No. 3, 2016, pp. 123-129.

[9] H. Hasegawa and S. Kimishima, "An investigation on working fluid selection of Rankine-Cycle driven by low grade heat with small temperature difference to environment", *Transactions of the Japan Society of Refrigerating and Air Conditioning Engineers*, Vol. 30, No. 1, 2013, pp. 1-12.

[10] P. A. Kew and K. Cornwell, "Development of a highly compact steam generator", *Applied Thermal Engineering*, Vol. 25, 2005, pp. 2604-2614.

[11] S. Tokuda and T. Osanai, "Exergie-Heat recovery analysis for exhaust gas in the boiler system", *Transactions of the Japan Society of Mechanical Engineers*, Series B, Vol. 50, No. 449, 1984, pp. 91-97.

[12] Xin, Z. Rao, X. You, Z. Song, D. Han, "Numerical investigation of vapor–liquid heat and mass transfer in porous media", *Energy Conversion and Management*, Vol. 78, 2014, pp. 1-7.

[13] Fei He, J. Wang, "Numerical investigation on critical heat flux and coolant", *Energy Conversion and Management*, Vol. 80, 2014, pp. 591-597.

[14] O. R. Alomar, M. A. A. Mendes, D. Trimis, S. Ray, "Numerical simulation of complete liquid-vapour phase change process inside porous media using smoothing of diffusion coefficient", *International Journal of Thermal Science*s, Vol. 86, 2014, pp. 408-420.

[15] O. R. Alomar, M. A. A. Mendes, S. Ray, D. Trimis, "Numerical investigation of complete evaporation process inside porous media using staggered and non-staggered grid arrangements", *International Journal of Thermal Sciences*, Vol. 129, 2018, pp.56-72.

[16] O. R. Alomar, R. R. Mohammed, M. A. A. Mendes, S. Ray, D. Trimis, "Numerical investigation of two-phase flow in anisotropic porous evaporator", *International Journal of Thermal Sciences*, Vol. 135, 2019, pp. 1-16.

[17] Lemmon, E. W., Huber, M. L. and Mc Linden, M. O., NIST REFPROP Ver.9 (2010).